# Effects of nanometric roughness on surface properties and fibroblast's initial cytocompatibilities of Ti6Al4V

Rex C.-C. Wang and Ming-Che Hsieh
*Institute of Manufacturing Engineering, National Cheng Kung University, Tainan 701, Taiwan*

Tzer-Min Lee[a)]
*Institute of Oral Medicine, National Cheng Kung University, Tainan 701, Taiwan*

(Received 20 April 2011; accepted 6 June 2011; published 8 July 2011)

Titanium alloy (Ti6Al4V) has widespread medical applications because of its excellent biocompatibility. Its biological responses can further be enhanced by polishing and passivation. Unfortunately, preparing titanium alloy samples of nanometric roughness is by far much more difficult than preparing those of micrometric roughness, and numerous investigations on roughness induced effects are all focused on micrometric scales. For the remedy, we investigate, at nanometric scale, the influence of roughness on surface properties and biological responses. Six groups of Ti6Al4V with average roughness ($R_a$) values of 2.75–30.34 nm are prepared. The results indicated that nanometric roughness of samples change the wettability and amphoteric OH groups. The contact angles monotonically decrease from 2.75 to 30.34 nm and the rougher surfaces lead to higher wettability. The *in vitro* cell-culture studies, using Murine NIH-3T3 fibroblasts, showed the spindle-shaped morphology on rougher surface compared to round/spherical morphology on smoother surface. A cytodetacher is employed to quantitatively measure the initial adhesion force of fibroblasts to specimen. The adhesion strength of fibroblasts, ranging from 55 to 193 nN, is significantly influenced by the nanometric roughness while the surface is within the range of 2.75–30.34 nm $R_a$ roughness, and the adhesion strength appeared stronger for rougher surface. The cell number on the smoother surface is higher than on the rougher surface at 5-day culture. The studies indicated that nanometric roughness would alter the surface properties and further influence cell morphology, adhesion strength, and proliferation. © *2011 American Vacuum Society*.
[DOI: 10.1116/1.3604528]

## I. INTRODUCTION

Titanium and titanium alloys, primarily Ti6Al4V, are widely used as dental, surgical, and other clinical implants[1,2] because of their excellent biocompatibility and mechanical properties. They form desirable passive oxide surface layers which impede the ion release rate and improve corrosion resistance.[3] While the interface is considered a key factor for good osseointegration, the surface properties of an implant, such as wettability, surface energy, topography, roughness and nanosurface compositions all combine to impact the initial cell responses.[2,4] Mechanical, chemical, and biological surface modification methods aimed at improving the bioactivity, biocompatibility, and corrosion resistance of titanium and titanium alloy were reported. For instance, Kim *et al.*[5] and Liu *et al.*[6] explored mechanical surface modification methods. They employed machining, grinding, and polishing to obtain specific surface topography and/or roughness. Rupprecht *et al.*[7] and Balamurugan *et al.*[8] explored chemical modification methods that applied chemical treatments such as chemical vapor deposition and sol-gel. In addition, biological surface modification methods were also reported that utilized RGD peptides, extracellular matrix proteins, and triamino acid sequence.[9,10] They were all set to creating biomimetic biomaterials that promote cell interactions with substrate.

Numerous investigations have concluded that, at micron and submicron scales, the surface roughness of titanium alloy influences the cell growth.[2,4] For example, Deligianni *et al.*[2] reported that the human bone marrow cells detect changes in Ti6Al4V roughness. Their results obtained at 0.320, 0.490, and 0.874 $\mu$m showed that the cellular attachment increases with roughness. Most molecular behaviors of living systems convey at nanometer scales. Consider type I collagen, one of the major organic components of bone. It is 300 nm long and 0.5 nm wide. Hydroxyapatite, one of the major inorganic components of bone, is only about 2–5 nm wide and 50 nm in length.[11] To extend the biological research from micron scale to the nanometric scale, Cai *et al.*[12] recently investigated the influence of roughness on protein adsorption and cell growth at nanometric scale. They coated titanium films on freshly cleaned glass slides using an electron-beam evaporator and achieved nanometer scale topography, where the specimens were grouped into surface roughnesses of $1.94 \pm 0.24$ nm, $10.27 \pm 0.45$ nm, and $20.73 \pm 2.68$ nm. Nevertheless, for titanium alloys, investigations of roughness impacts on cell growth are still bundled at micron and submicron scales. The nanometric efforts were not expanded beyond coated titanium film and extended further to the titanium alloy. There is an urgent need to fill the "nanometric" gap.

[a)]Electronic mail: tmlee@mail.ncku.edu.tw

 1934-8630/2011/6(3)/87/11/$30.00  

Previously, we investigated the effects of passivation treatments on titanium alloy, where the biological responses of fibroblasts' initial adhesion were examined on the individual basis.[13] The passivation treatments not only modified both roughness and nanosurface chemical property of titanium alloy, but also changed initial cell morphology and initial adhesion force. The observed changes in initial adhesion force and roughness revealed that the biological behavior of fibroblasts is influenced by changes in roughness, a conclusion supported by Deligianni *et al.*[2] for human bone marrow cells. Here, the changes in roughness are refined down to the nanometric scale. It was also observed that the initial adhesion force of fibroblasts is correlated to OH basic groups. In fact, instead of being independent, the passivation effects on roughness and nanosurface chemical property are paired for each treatment. Thus, the influence of roughness on the cell's initial response cannot be isolated from passivation treatment. It is necessary to further investigate the effect of roughness changes at nanometric scale on the surface properties and cell responses. This study is intended to correlate nanometric roughness–wettability–amphoteric OH content of titanium alloy (Ti6Al4V) and attempts to unveil the influence of nanometric roughness on initial cell adhesion force, cell morphology, and cell proliferation.

## II. MATERIALS AND METHODS

### A. Experimental materials

Surgical grade Ti-6A1-4V alloy (ASTM F136-92) disc plates, measuring 12.7 mm in diameter and 2 mm in thickness, are applied. To obtain the desired surface roughness ranging from 2 to 30 nm as measured by $R_a$ values, they were ground by a sequence of wet grindings using grit silicon carbide papers of 320, 400, 600, 800, 1000, 1200, and 1500 grit in the stated order for the rougher groups. It controlled the rotation rates, grinding time, and downward force of the automatic grinder (Ecomet3, Buehler). For the rougher groups, the more rapid rotation rates, shorter times, and higher forces were needed. For the smoother surfaces, the parameters of the rotation rates and downward force were gradually reduced, but the process needed the longer grinding time. The grinding operations were followed by another procedure of polishing using $Al_2O_3$ powder of 5, 1, and 0.3 $\mu$m. This simple method can be used to modify the surface topographies and $R_a$ values, and to achieve the desired roughness. Thus, six specific procedures were used to prepare the six specific roughness classes. Hereafter, these six groups of samples are labeled HT1, HT2, HT3, HT4, HT5, and HT6 samples. Then, the Ti6Al4V plates were further passivated by oxidizing at 400 °C in atmosphere furnace for 45 min. Then, they were ultrasonically cleaned in 95% ethanol and three times in de-ionized water right before being packed in double-sealed autoclaving bags, which were autoclaving at 121°C for 30 min and dried at 121°C for 15 min.

### B. Surface characterization

An scanning probe microscopy [(SPM), IIIa DimensionTM 3000, Digital Instruments Inc., USA], set in tapping model and operated at ambient temperature, was employed while taking $R_a$ values and the topography details, all down to the nanometer scale. The $R_a$ value of a scanned area is defined as the average height of the center line, or average of the absolute heights of all points in the profile. The $R_a$ parameter is calculated using

$$R_a = \frac{1}{L_x L_y} \int_0^{L_y} \int_0^{L_x} |f(x,y)| dx\, dy, \tag{1}$$

where $f(x, y)$ is the surface relative to the center plane and $L_x$ and $L_y$ are the length of roughness curve.[14]

Wettability, regularly represented by the contact angle of a droplet freshly put on the tested surface,[15] is considered one of the important surface properties. The sessile drop method has been employed. It measures the contact angles of double distilled water drops using a contact angle meter manufactured by FACE CA-A, Kyowa Interface Science Co., Japan. Contact angles of double distilled water drops were measured at room temperature for HT1–HT6 samples. Five specimens were randomly selected from each group, and five contact angles were obtained at randomly selected spots for each specimen.

Surface chemical analyses have been carried out using x-ray photoelectron spectroscopy [(XPS), Axis Ultra DLD, Kratos Analytical Co., UK], operated at 12 kV and 20 mA at a pressure less than $10^{-8}$ mbar, using Mg $K\alpha$ radiation. Measurements of binding energy in the range 0–1000 eV were made at a "take-off" angle of 45° with respect to the sample surface. High-resolution scan of oxygen peak was performed on selected specimens. The binding energy was calibrated by C 1*s* peak at 284.6 eV. The data were analyzed by XPSPEAK 4.1 software to decompose the overlapping peaks.

### C. Cell culture

The Murine NIH-3T3 fibroblasts cultured on discs of HT1–HT6 groups were examined. One disc per well, the discs were placed in a well plate which holds up to 24 discs. Then, fibroblasts with an initial density of $10^4$ cells per milliliter were seeded on the discs. The Murine NIH-3T3 fibroblasts were cultured in Dulbecco's modified Eagle's medium (DMEM; Gibco) supplemented with 10% bovine serum (BS; Gibco), 0.06 mg/ml penicillin (Sigma), 0.1 mg/ml streptomycin sulfate (Sigma), and 3.7 mg/ml $NaHCO_3$ (Sigma). The cells were maintained in an incubator equilibrated with 5% $CO_2$ at 37 °C. Fresh medium were added every other day until harvesting.

### D. Cell morphology

Scanning electron microscopy (SEM) was employed to examine the cell morphology, where the fibroblasts were

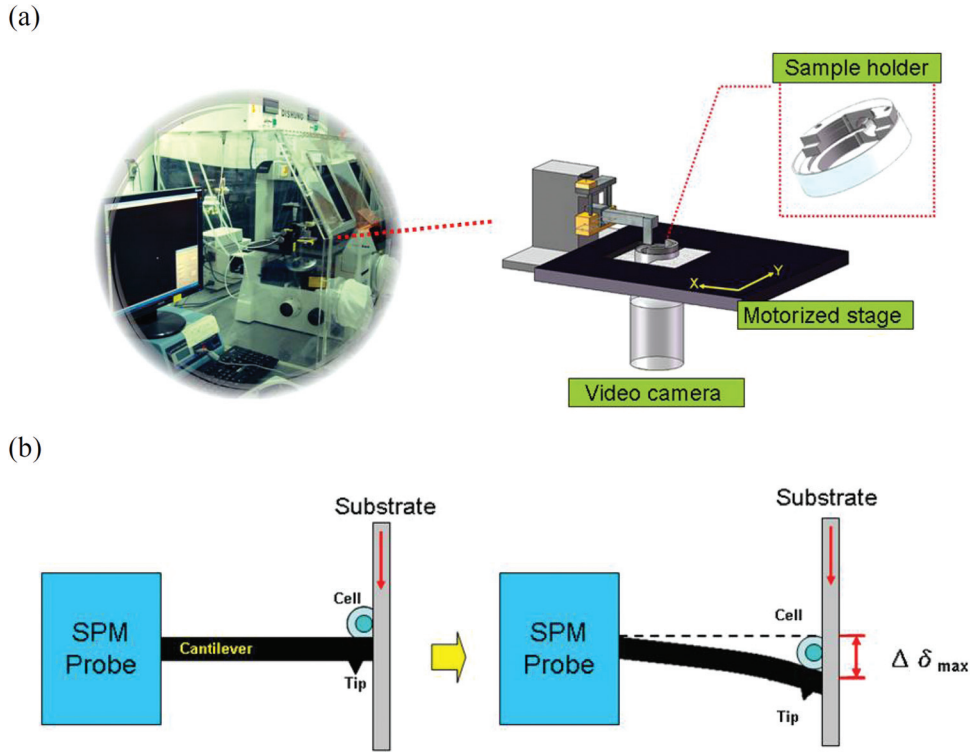


FIG. 1. (Color) Illustrations of the fixture, sample holder, and cell detachment by an SPM cantilever. (a) Major components of the cytodetacher apparatus. (b) The cells as viewed in the video camera and displaced by the SPM cantilever.

cultured in DMEM containing 10% BS in 37 °C and 5% $CO_2$ for 3 and 24 h. At harvest point, the medium were removed and gently rinsed three times with phosphate buffered saline (PBS). The discs were fixed with 2.5% glutaraldehyde for 30 min. Then, they were rinsed with PBS again before postfixing in 1% osmium tetroxide ($OsO_4$). After washing the fixation by PBS, the discs were sequentially dehydrated in 30%, 50%, 75%, and 100% ethanol, each immersed three times for 1 min. Finally, the discs were soaked in HMDS for 30 min, and platinum coated using a sputter coater and observed by SEM (XL40FEG, Philips, The Netherlands).

### E. Cytodetachment test

Fibroblasts with cell density of $5 \times 10^3$ cells/ml were seeded on the substrate and cultured for 3 h before being subjected to scraping. A cytodetacher was employed to quantitatively measure the adhesion strength of an individual cell. The cytodetacher was built on the microscope working station of laser tweezers (Cell Robotics Inc, Albuquerque, NM). As shown in Fig. 1(a), it consists of four components: (1) the SPM probe (MikroMasch, CSC38/A1BS) with spring constant 0.0129 N/m, (2) the cell selector, (3) the sample holder, and (4) the microscope working station equipped with a motorized stage, a video camera, and a microscope (Nikon, model TE300). Figure 1(b) shows that the SPM probe is fixed on the cell selector, and cells are seeded on a substrate. While the motor stage is moving in the $x$ direction, the cantilever of the SPM probe scrapes the individual cell. Digital images of the scraping process were recorded. Let $F_{\text{adhesion}}$ and $\delta_{\max}$ be the cell adhesion force and the maximal deflection at the cantilever's tip, respectively. The value of $\delta_{\max}$ in each scraping was identified from the recorded images, and the adhesive force was obtained using Hooke's Law as follows:[13]

$$F_{\text{adhesion}} = K\delta_{\max}, \tag{2}$$

where $K = 0.0129$ N/m is the spring constant of the cantilever.

### F. MTT cell proliferation assay

The proliferation rates of Murine NIH-3T3 fibroblasts cultured on discs of HT1–HT6 groups for 1, 3, and 5 days were examined. The MTT [3-(4,5-Dimethylthiazol-2-yl)-2,5- diphenyltetrazolium bromide, Sigma, St. Louis, MO)] assay, a standard colorimetric method for measuring the proliferation rates of cells, was employed. At the harvesting of Murine NIH-3T3 fibroblasts, 200 $\mu$l of MTT working solution was added to every well, and the cells were incubated for 4 h in 5% $CO_2$ at 37 °C. Then, the well was drained using a pipette and refilled with 1 ml dimethyl sulfoxide before putting on a waver shaker (MW-23, Major Science, ROC). After 30 min of shaking, the absorbance was measured using an enzyme-linked immunosorbent assay (ELISA) plate reader (TECAN, SUNRISE) with a wavelength of 562 nm.

TABLE I. Average $R_a$ values and contact angles of specimens with autoclaving treatment.

(a) $R_a$ values for HT group

| Specimens | Mean (nm) | SD (nm) | $\sigma/\mu$ (%) |
|---|---|---|---|
| HT1 | 30.34 | 2.69 | 9 |
| HT2 | 20.84 | 2.26 | 11 |
| HT3 | 11.72 | 2.04 | 17 |
| HT4 | 5.26 | 0.48 | 9 |
| HT5 | 3.98 | 0.33 | 8 |
| HT6 | 2.75 | 0.22 | 8 |

(b) Contact angle for HT group

| Specimens | Mean (deg) | SD (deg) | $\sigma/\mu$ (%) |
|---|---|---|---|
| HT1 | 83.12 | 4.25 | 5 |
| HT2 | 88.88 | 4.66 | 5 |
| HT3 | 91.28 | 5.74 | 6 |
| HT4 | 92.32 | 5.12 | 6 |
| HT5 | 95.60 | 2.52 | 3 |
| HT6 | 97.68 | 2.81 | 3 |

### G. Statistical analysis

Each data point represents the mean ± standard deviation (SD) of the surface roughness, static contact angle, proliferation rates, and cell adhesive force. The unbalanced design of randomized tested one-way analysis of variance (ANOVA) was employed to test the significant differences among cell adhesive strengths of HT1, HT2, HT3, HT4, HT5, and HT6 treatments. Duncan test at the significance level of 0.05 was carried out to group magnitudes of treatment effects.

## III. RESULTS

### A. Surface characterization

#### 1. Surface topography (SPM)

Six groups of samples with distinct roughness were prepared using the procedure described in Sec. II A. Table I lists their mean $R_a$ values and standard deviations. Their mean $R_a$ values, as measured by the same SPM, are separately 30.34, 20.84, 11.72, 5.26, 3.98, and 2.75 nm. Hereafter, these six groups of samples are labeled the HT1, HT2, HT3, HT4, HT5, and HT6 samples. Figure 2(a) shows the scatter chart of $R_a$ values for randomly taken samples. Duncan's test was conducted, and the significance level was set at 0.05. Results are shown in Fig. 2(b). Duncan's test concludes that the roughness of every HT group does significantly differ from all others.

While determining the average $R_a$ values of discs for the HT1–HT6 groups, five discs were taken randomly from each group, and $R_a$ measurements were taken at five randomly selected spots per disc. The average $R_a$ values ($\mu$) of all six groups and their standard deviations are summarized in Table I, where the corresponding standard deviations ($\sigma$) and the $\sigma/\mu$ ratios are also listed, and the $\sigma/\mu$ ratios are displayed in percentages (%). It is observed that, from top down, the magnitude of standard deviation decreased about ten times as the mean values also declined about ten times. It appears that the magnitude of standard deviation proportionally decreased with the magnitude of mean value. In addition, the $\sigma/\mu$ ratios appeared to be around 12.5% and fluctuated within a rather narrow range, from 8% to 17%, and they are uncorrelated with the magnitude of mean values.

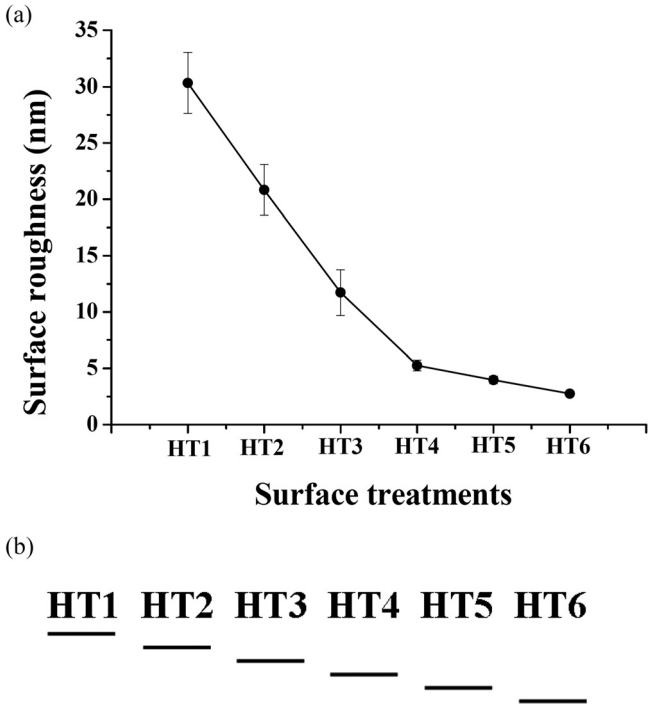


FIG. 2. Measurements of surface roughness and Duncan grouping. (a) Measurements of $R_a$, (b) Duncan grouping of $R_a$.

Figures 3 and 4 present the surface topographical images of the specimens acquired by 5 $\mu$m × 5 $\mu$m SPM scans and the height of the $Z$ direction was 600 and 100 nm, respectively. As shown in Fig. 4, the surfaces of both HT1 and HT2 contain valleys and hills. The surface of HT3 exhibits shallow grooves. The surfaces of the remaining three groups, i.e., HT4–HT6, share a similar appearance, and all of them contain unevenly scattering bumps. By visual inspection; still we can tell that from HT4 to HT6 the bumps reduce in magnitude, but not in number.

#### 2. Contact angle

Measurements of static contact angles are shown in Fig. 5(a). The wettability monotonically decreases from HT1 to HT6. HT1 has the smallest contact angle of 83.17° while HT6 has the largest contact angle of 97.68°. Thus, the HT1 sample has the highest wettability, and the HT6 has the lowest wettability. Duncan's test was conducted at the significance level of 0.05. Figure 5(b) shows the results, where the bold lines beneath (HT2, HT3), (HT3, HT4), and (HT5, HT6) denote that the difference in wettability between the paired specimens of (HT2, HT3), (HT3, HT4), and (HT5,

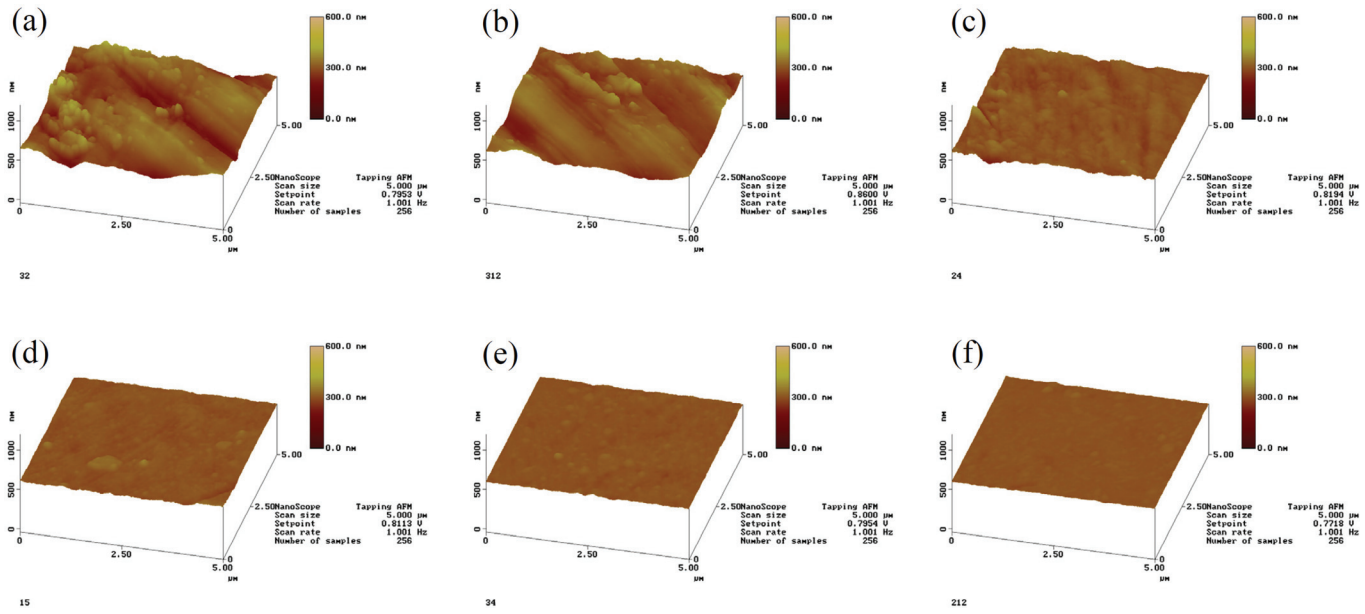


FIG. 3. (Color) Surface topography of samples acquired using 5 $\mu$m × 5 $\mu$m SPM scans and height image ($Z$ range 600 nm). (a) HT1, (b) HT2, (c) HT3, (d) HT4, (e) HT5, and (f) HT6 specimens.

HT6) is statistically insignificant and that the differences among all other specimen pairs are statistically significant. Let $\mu_{CA}(HTi)$ be the mean value of the contact angles obtained for samples of the HT$i$ group, $i = 1$–6. Conduct the two-sample t-test for $H_0 : \mu_{CA}(HT2) = \mu_{CA}(HT3)$ vs $H_1 : \mu_{CA}(HT2) \neq \mu_{CA}(HT3)$ resulting in a $p$ value of 0.1111. Test $H_0 : \mu_{CA}(HT3) = \mu_{CA}(HT4)$ vs $H_1 : \mu_{CA}(HT3) \neq \mu_{CA}(HT4)$ resulting in a $p$ value of 0.5023, and testing $H_0 : \mu_{CA}(HT5) = \mu_{CA}(HT6)$ vs $H_1 : \mu_{CA}(HT5) \neq \mu_{CA}(HT6)$ produces a $p$ value of 0.0082. It is noted that, with the exception of (HT2, HT3) and (HT3, HT4) pairs, all the differences among contact angles of HT1–HT6 were statistically significant.

### 3. XPS analyses of sample

Three oxygen-containing species are absorbed on the sample surface, namely, the nanosurface compositions of O 1$s$, OH acidic, and basic Ti–OH groups. Percentages of the three oxygen specimens are listed in Table II for all the HT samples. It is observed that, by increasing the surface roughness, the percentages of basic Ti–OH group increase from

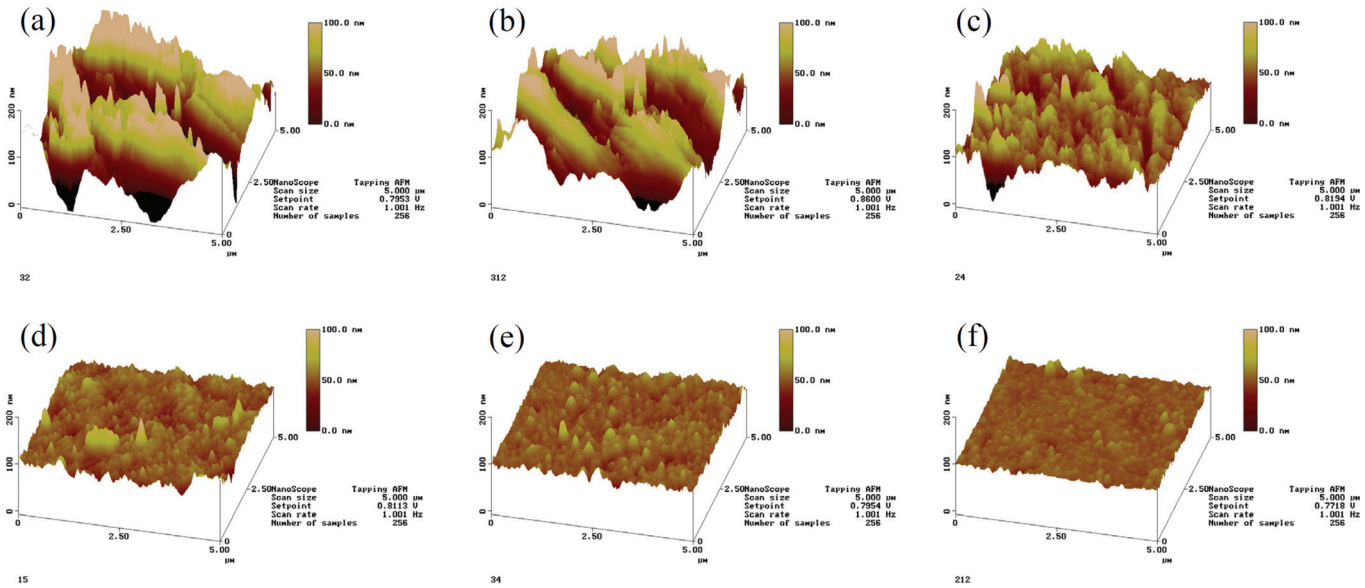


FIG. 4. (Color) Surface topography of samples acquired using 5 $\mu$m × 5 $\mu$m SPM scans and height image ($Z$ range 100 nm). (a) HT1, (b) HT2, (c) HT3, (d) HT4, (e) HT5, and (f) HT6 specimens.

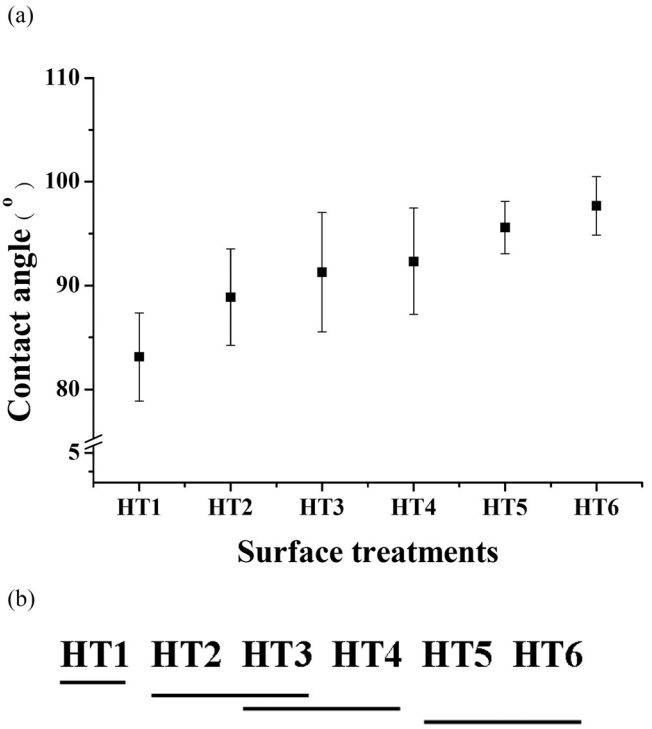


FIG. 5. Measurements of static contact angle and Duncan grouping. (a) Measurements of contact angle, (b) Duncan grouping of contact angle.

5.6% of HT6 to 8.3% of HT1 while the surface roughness increases from 2.75 nm of HT6 to 30.34 nm of HT1. The percentage of OH acidic groups increases from 15.5% of HT6 to 22.1% of HT1.

## B. Cell culture studies

### 1. Cell morphology

As shown in Fig. 6, cells are cultured for 3 h and imaged by the scanning electron microscope. It is observed that the cells appear to adopt a spindle shape on the rough surfaces of HT1 and HT2 specimens as shown in Figs. 6(a) and 6(b). The cells share a more round/spherical morphology on the smooth surfaces of HT3, HT4, HT5, and HT6 specimens as shown in Figs. 6(c)–6(f). Three phenotypes are distinguished, namely, full spread, partial spread, and no spread. In the full spread, the cell has extension of plasma membrane to all sides, combined with distinctly larger surface area and obvious flattening. As shown in Figs. 6(a) and 6(b), cells on HT1 and HT2 are in full spread, and the cell on HT1 has fuller spreading than the one on the HT2. In the partial spread, cells begin to spread laterally at one or more sides, but the extensions of plasma member are not completely confluent. As shown in Figs. 6(c)–6(e), cells on HT3, HT4, and HT5 are all in partial spread, where the differentiation among those cell morphologies is minor. In the no spread, the cell still appears spherical, and no lamellipodia is yet produced as the cell shown in Fig. 6(f). Figure 7 contains pictures of cells cultured for 1 day and imaged at 3000× magnification. The fibroblasts, after 1-day culturing, appear larger than those cultured for 3 h, and lamellipodia and filopodia have been clearly developed. A close look reveals that cells cultured on HT1, HT2, HT3, HT4, and HT5, display well-developed filopodia and lamellipodia. The spreading is less pronounced for cells on the HT6 group.

TABLE II. High-resolution XPS surface chemical analyses (at. %) of oxygen spectra for specimens with autoclaving treatment.

| Specimens | Ti–OH basic (%) | OH acidic (%) | O 1*s* (%) |
|---|---|---|---|
| HT1 | 8.3 | 15.5 | 76.2 |
| HT2 | 8.2 | 18.6 | 73.2 |
| HT3 | 7.6 | 20.0 | 72.4 |
| HT4 | 7.1 | 20.8 | 72.1 |
| HT5 | 6.2 | 21.0 | 72.8 |
| HT6 | 5.6 | 22.1 | 72.3 |

### 2. Initial cell adhesion force

The average adhesive forces of individual fibroblasts are 193, 148, 134, 109, 107, and 55 nN for HT1, HT2, HT3, HT4, HT5, and HT6, respectively. Results of one-way ANOVA reveal that the group difference is statistically significant with a $p$ value less than 0.0001. The Duncan test is conducted at the significance level of 0.05. Figure 8(a) displays the results. While in Fig. 8(b), the bold line beneath HT2, HT3, HT4, and HT5 indicates that their adhesive forces do not differ from each other significantly, the adhesive forces of HT1, HT6, and every member of the HT2, HT3, HT4, and HT5 group are statistically different from each other.

### 3. Cell proliferation

The MTT cell proliferation tests are carried out for all the six groups. The bar chart of Fig. 9(a) displays the cell numbers, where it is observed that the cell numbers increase for 1, 3, and 5 days, and reach their peaks in 5 days. Figures 9(b) and 9(c) show Duncan test results for 1 and 3 days. No significant differences are observed among those six groups. Figure 9(d) contains Duncan test results for 5 days, where one bold line lies beneath HT1, HT2, and HT3, and another one lies beneath HT2, HT3, HT4, HT5, and HT6. The Duncan test indicates that while the cell number of HT1 statistically differs from those of HT4, HT5, and HT6, all other paired cell numbers are considered statistically indistinguishable.

## IV. DISCUSSION

Previous investigations have reported that the wettability increases with roughness. Lawrence *et al.* (2006) applied a Nd:YAG laser to modify the surface of a Ti6Al4V alloy and measured the $R_a$ value using a surface profilometer (Surface tester SV-600; Mitutoyo, Inc.),[16] where the unmodified surface roughness was averaged at 0.21 $\mu$m, and the post-treatment roughness was 0.45 $\mu$m. It was found that the laser-

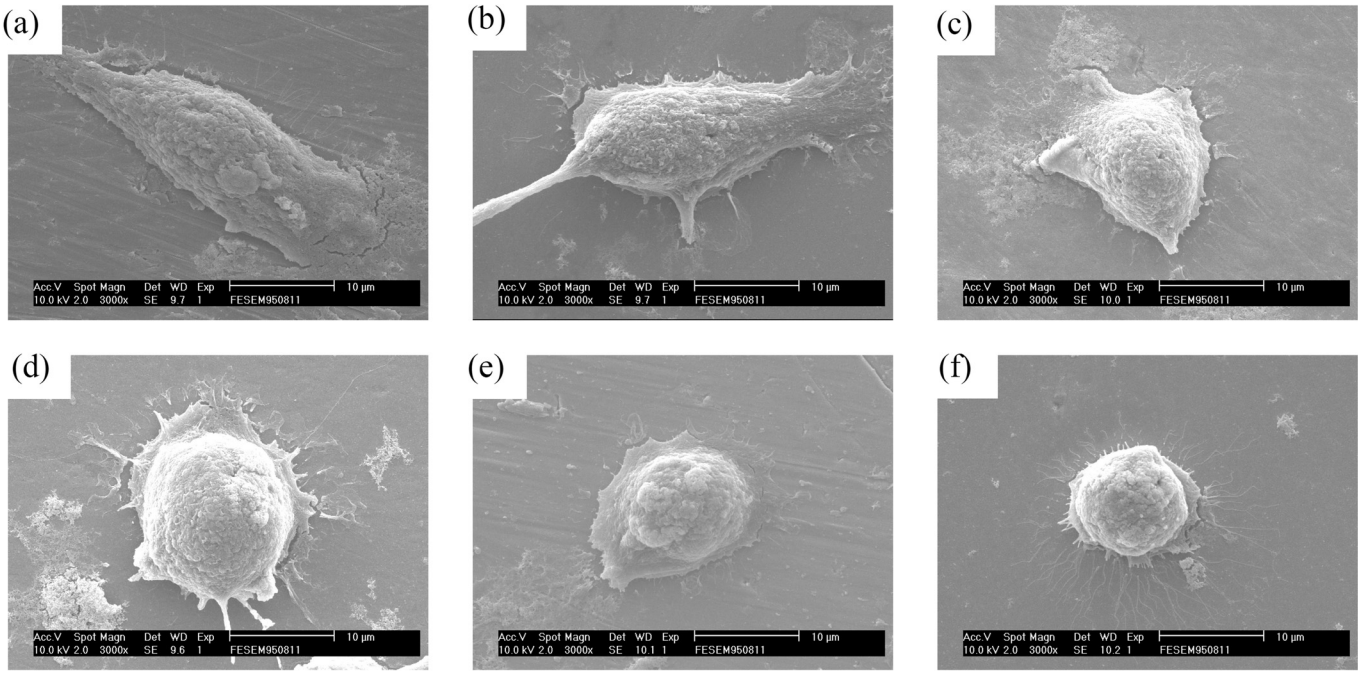


FIG. 6. Scanning electron micrographs of NIH-3T3 fibroblasts that have been cultured for 3 h on (a) HT1, (b) HT2, (c) HT3, (d) HT4, (e) HT5, and (f) HT6 specimens.

induced increase in surface roughness also raises the wettability. While numerous studies achieved results at micron scale, only one investigation reporting results evaluated for coated nanostructured $TiO_2$ films on glass substrates. Attempting to extend that effort from micron scale to nanometric scale, Zhou *et al*. coated nanostructured $TiO_2$ films on glass substrates, and achieved surfaces with rms roughness ranging from about 5 to 20 nm as measured by an AFM.[17] It was observed that a rougher surface has a smaller contact angle. Thus, at the nanometric scale raising the surface roughness increases the wettability, similar to results observed in the micron scale. To further the investigation beyond coated nanostructures, we have studied Ti6Al4V that was polished and passivated to have nanoroughness.

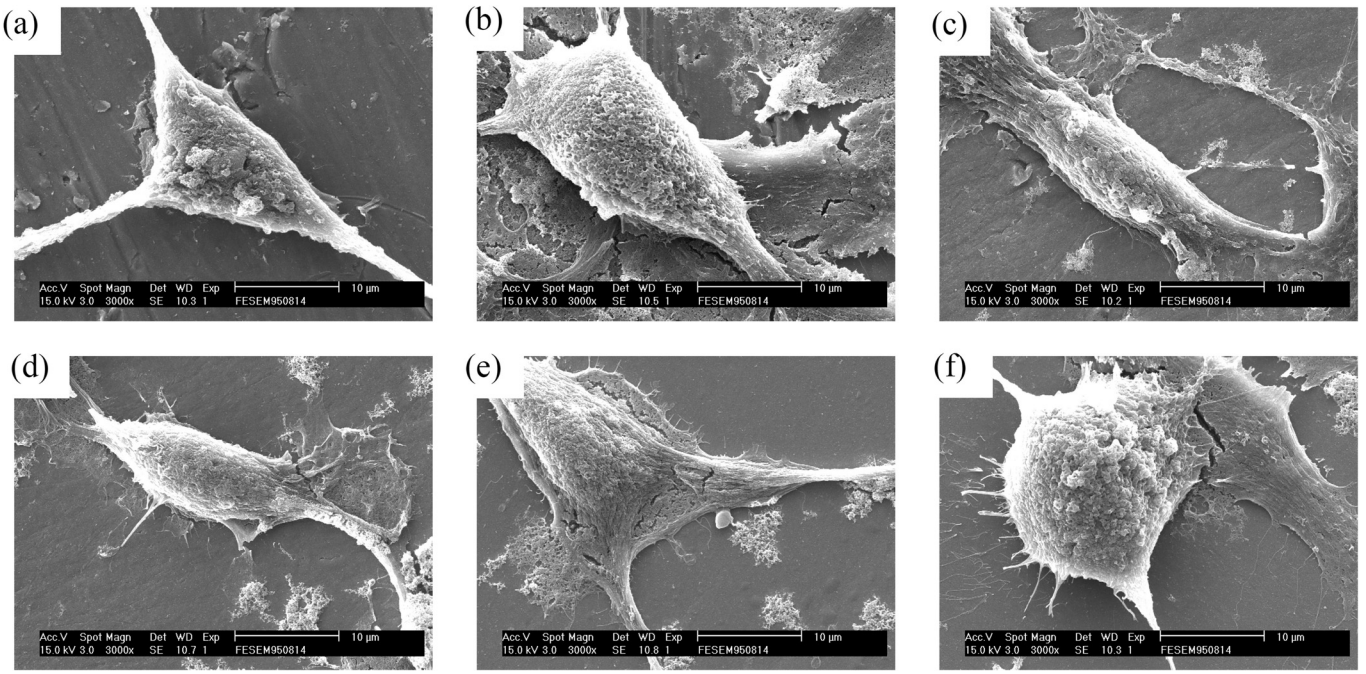


FIG. 7. Scanning electron micrographs of NIH-3T3 fibroblasts that have been cultured for 1 day on (a) HT1, (b) HT2, (c) HT3, (d) HT4, (e) HT5, and (f) HT6 specimens.

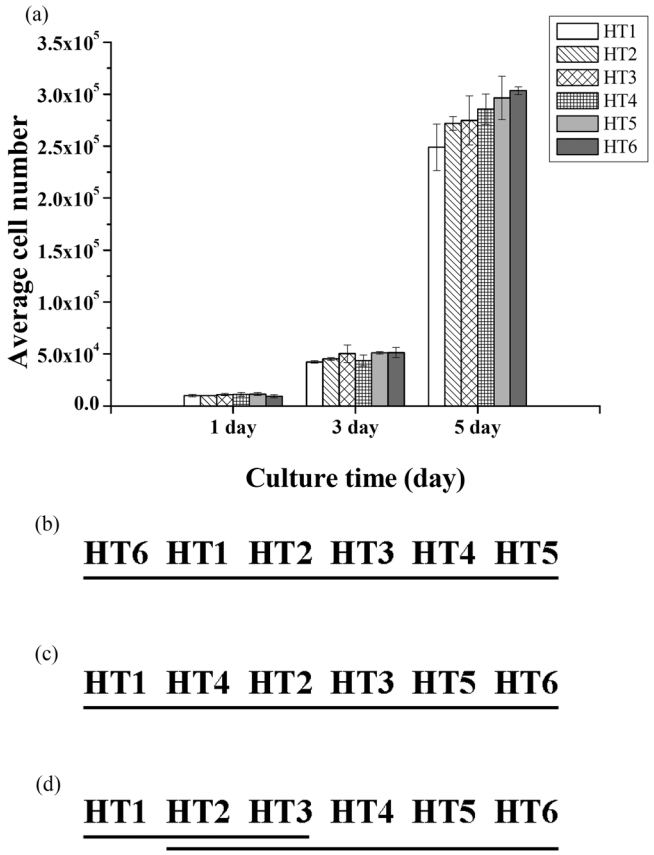


FIG. 8. Measurements of cell adhesion force and Duncan grouping. (a) Measurements of cell adhesion force, (b) Duncan grouping of cell adhesive force.

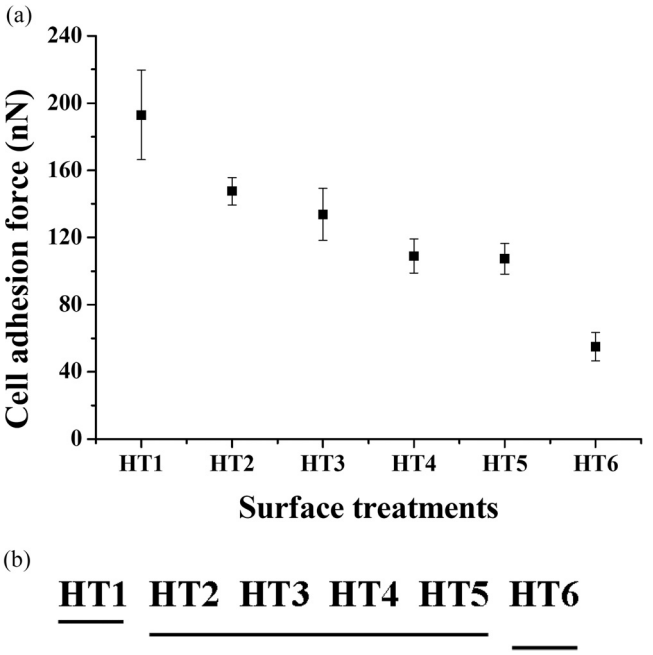


FIG. 9. Results of MTT cell proliferation assay for 1, 3, and 5 days on HT1–HT6 specimens. The bar chart shows the mean and standard deviations of the cell numbers; $n=3$ and Ducan groups of MTT analysis for 1, 3, and 5 days. (a) Measurements of MTT cell proliferation assay, (b) Duncan grouping of 1-day MTT assay, (c) Duncan grouping of 3-day MTT assay, and (d) Duncan grouping of 5-day MTT assay.

The mean $R_a$ values of HT1–HT6, as listed in Table I, are, respectively, 30.34, 20.84, 11.72, 5.26, 3.98, and 2.75 nm. Figure 5(a) contains their contact angles, where it is observed that the contact angles monotonically increase from HT1 to HT6. Since the roughness decreases from HT1 to HT6 and high contact angle corresponds to low wettability, our results show that the wettability increases with roughness, which is consistent with previous findings. Further examination for the contact angles and the $R_a$ values contained in Table I reveals that the contact angle monotonically increases from HT1 to HT6 while the corresponding surface roughness monotonically decreases as well. Both monotonic trends suggest the existence of negative correlation between contact angle and roughness. To find out the statistical significance of the anticipated negative correlation, we applied SAS CORR Procedure that yields a Pearson correlation coefficient ($r_P$) of $-0.95788$, where the $p$ value associated with testing the null hypothesis of $H_0 : r_P = 0$ is 0.0026. Thus, the negative correlation between wettability and roughness is statistically significant. The above-presented findings are in line with previously reported results regardless of the nanometric or micron scale roughness, and Ti6Al4V alloy or $TiO_2$ coated glass surface. Further considerations that support the observed negative correlation are addressed in the following.

The contact angle is a function of the surface energy, which is the amount of energy required to disrupt the intermolecular bonds that occur when a surface is created. The well-regarded Young's equation describes the balance among forces experienced by the droplet on a dry surface as follows:

$$\gamma_{sl} = \gamma_{sv} - \gamma_{lv} \cos\theta_w, \tag{3a}$$

where $\gamma_{sl}$, $\gamma_{sv}$, and $\gamma_{lv}$ are the interfacial tensions between the solid and the liquid, the solid and the vapor, and the liquid and the vapor, respectively, and $\theta_w$ denotes the equilibrium contact angle that the droplet makes with the surface. The Young's equation assumes a perfectly flat surface. Unfortunately, it is rarely true in the real world. Surface roughness and impurities exist, and they might cause a deviation from the equilibrium predicted by the above-presented Young's equation. The following Wenzel's equation[16] takes roughness into consideration:

$$\gamma_{sl} = \gamma_{sv} - \left(\frac{\gamma_{lv} \cos\theta_w}{r}\right), \tag{3b}$$

where the surface roughness, denoted by $r$, is given by the ratio of real and apparent surface areas. The interfacial tensions in Young's equation are material properties, and they are dependent on the materials only, including the material that makes the solid, the liquid, and the vapor. Therefore, those values of $\gamma_{sl}$, $\gamma_{sv}$, and $\gamma_{lv}$ should remain fixed unless the composition of material is modified. Thus, the Wenzel's

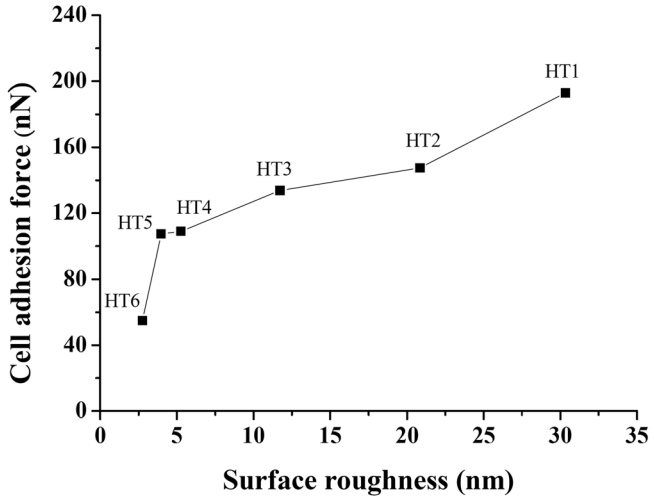


FIG. 10. Comparsion of $TiO_2$ structure between HT1 and HT6.

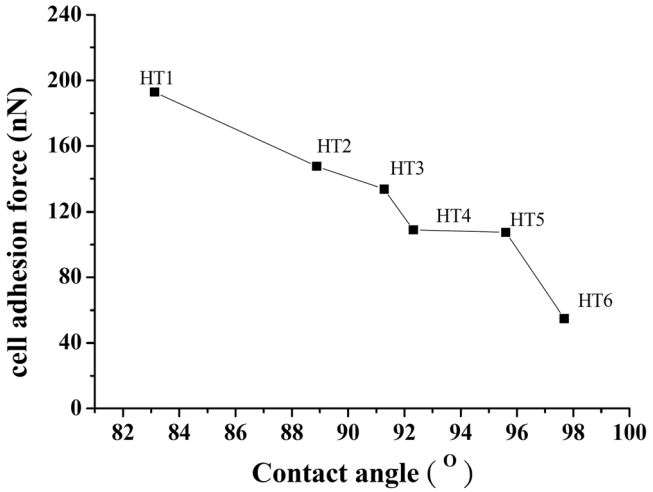


FIG. 11. Relationship between roughness and cell adhesion force.

equation observes the following situation: reducing $r$ raises $\theta_w$. That is, a smoother surface has a smaller $r$ and; consequently, a larger equilibrium contact angle. The above-presented conclusion is in line with what we observed in the last paragraph.

Previously, Bandura *et al.* (2004) discussed the $H_2O$–$TiO_2$ (rutile) interface. They reported that the probability of $H_2O$ dissociation is decreased with decreased surface coverage (or decreasing roughness). One explanation of this change in mechanism with reduced coverage is that $H_2O$ molecules can readily align to provide the maximum H-bonding interaction in associatively adsorbed structures. At low coverage, H-bonding energies are not as significant as at a higher coverage, so the additional energy of forming stronger Ti–OH bonds outweighs the H-bonding term.[18] As a consequence, low coverage comes with low wettability, or equivalently high coverage with high wettability. In this study, the substrate was passivated by oxidizing at 400 °C in atmosphere, and the $TiO_2$ forms the primitive tetragonal unit cell of rutile, with unit cell parameters $a = 4.594$ Å, and $c = 2.959$ Å. Compare the surface topographical images of HT1 groups with HT6 groups of Fig. 4, and we observe the surface of HT1 appears to contain more relatively conspicuous valleys than those of HT6. Therefore, HT1 has higher coverage. Thus, the rougher surface comes with more surface coverage area. On the other hand, the percentage of Ti–OH groups decreases from 27.7% of HT6 to 23.8% of HT1, while the surface roughness increases from 2.75 nm of HT6 to 30.34 nm of HT1. Thus, a rougher surface has higher coverage, adsorbs more $H_2O$, and has higher wettability. Our results are consistent with those of Bandura *et al.*

Both shape and dimension of grooves on the substrate surface influence cell morphology and adhesion. Previously, Ponsonnet *et al.* found that cells would orient in a parallel order along the grooves caused by mechanical polishing. In contrast, they appeared to grow with no specific orientation on smooth surface.[19] Therefore, a rougher surface with grove topography affected the cell morphology. In 2009, Chen *et al.* showed that RGD tripeptide attaches to the grooved surface through carboxyl oxygen atoms in both Asp backbone and side chain. Grooved surface is shown to provide higher reactivity adsorption sites, thereby forming a more stable adsorption state than that onto the perfect surface.[20] As shown in Fig. 4, the surfaces of the roughest groups contain grooves. Those grooves could have reinforced the fibroblast attaching to the surface of titanium alloy and strengthened the adhesion force. Figure 10 plots the adhesive force of fibroblasts versus the nanometric $R_a$ roughness. It is observed that the adhesive force monotonically increases with surface roughness.

Figure 11 plots the cell adhesion force against the contact angle. It is observed that the adhesive force monotonically decreases as the contact angles increases, or equivalently the adhesive force monotonically increases with the wettability. Previously, researchers measured the adhesive fore of Murine fibroblast on the glass dish. They reported that cell-material adhesion is affected by the material's surface charge density, hydrophilicity/hydrophobicity, and wettability.[21,22]

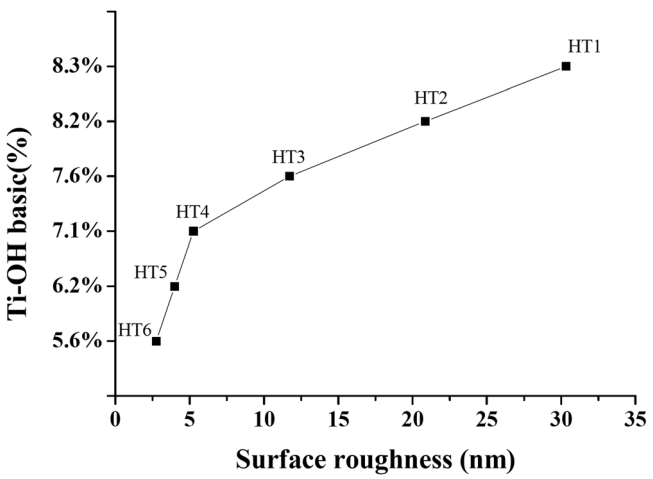


FIG. 12. Relationship between contact angle and cell adhesive force.

Their findings revealed that high wettability material favors cell adhesion. In a different development, Sagvolden and coworkers cultured human cervical carcinoma cells on hydrophilic and hydrophobic specimens. Their results show that cervical carcinoma cells attached faster and better on a hydrophilic substrate than a hydrophobic one.[23,24] Our results are consistent with the above-presented findings, and fibroblasts adhere stronger on discs of higher wettability.

The hydrated titanium oxide layer of $TiO_2$ is known to have at least two types of hydroxyl groups: acidic OH with oxygen doubly coordinated to titanium, and basic Ti–OH group singly coordinated. Feng *et al*. found that the Ti–OH basic groups would raise positive charges on titanium alloy's surfaces, and the $OH_a$ groups would give rise to negatively charged surfaces.[25] In addition, Weeb *et al*. reported that the positively charged surface promotes NIH-3T3 fibroblast attachment and spread.[21] As revealed in Figure 12, the Ti–OH basic increased with the surface $R_a$ roughness. This could be explained by the fact that the rough samples could provide more sites with Ti readily available for coordinating the $OH^-$ group. Therefore, the rougher surface is more positively charged, and our finding is consistent with the reported ones. Table II displays that the rougher surfaces contain higher percentages of basic Ti–OH, which gives rise to positively charged surfaces. Since the positively charged surface promotes NIH-3T3 fibroblast attachment and spread, initial cell adhesion would be stronger on rougher surfaces. Our results confirm that cells cultured for 3 h on rougher surfaces would have fuller spread than those on smoother surfaces. In addition, the measured initial adhesion strengths are positively correlated with the surface $R_a$ roughness.

Correlation between cell numbers and surface roughness was analyzed using SAS CORR Procedure, and Pearson correlation coefficients and $p$ values were obtained. It is observed that all the sample correlations are negative and, with the exception of 1 day, all the $p$ values are less than 0.05. Thus, the cell proliferation rates and the $R_a$ surface roughness are considered negatively correlated, i.e., the Murine NIH-3T3 fibroblasts multiply faster on smoother surfaces. Previously, Ponsonnet *et al*., investigated the influence of NiTi alloy roughness on the proliferation of fibroblasts, where the peak-to-valley ($Rz$) roughness ranged from about 0.5 to 6 $\mu$m as measured by a perthometer. Their results showed that the optimal density values increased while the surface roughness decreased.[26] Thus, our results further evidenced that fibroblasts multiply faster on smoother surfaces down to nanometric scales.

## V. CONCLUSION

This study demonstrates that Ti6Al4V surface roughness at nanometric scale affects surface properties and cell compatibility. $R_a$ roughness of HT1–HT6 specimens monotonically decreases from 30.34 to 2.75 nm. The nanosurface properties and cytocompatibilities of 400 °C passivation samples have been examined. The results lead to the following conclusions.

(1) The contact angles monotonically increase from HT1 to HT6. HT1 has the smallest contact angle of 83.17° while HT6 has the largest contact angle of 97.68°.
(2) The percentage of basic Ti–OH groups monotonically decreases from 8.3% of HT1 to 4.6% of HT6.
(3) The initial cell adhesive force monotonically decreases from 193 nN of HT1to 55 nN of HT6.
(4) The 5-day proliferation rates monotonically increase from HT1to HT6.
(5) After 3 h, culturing cells on rougher surfaces appear to be spindle-shaped while cells on smoother surfaces share a more round/spherical morphology.

Judging from the initial cell adhesion strength and the initial cell behavior, we conclude that, for surfaces within the range of 30.34–2.75 nm $R_a$ roughness, the roughness would influence the cell behavior even down to nanometric scales. Thus, these surface properties, topography, chemical composition, and wettability may be useful for the determination of clinically desirable implant surfaces. Surface roughness at nanometric clearly affects fibroblast adhesion and proliferation and should be considered in future implant design.

## ACKNOWLEDGMENTS

This work has been partially financed by National Science Council, Taiwan, under NSC 97-2221-E-006-079-MY3 and NSC 97-2221-E-006-005-MY2. The authors also appreciate the support from the Center for Frontier Materials and Micro/Nano Science and Technology (CFMMNST), National Cheng Kung University, Taiwan (D98-2700). Shih Ping Yang and Fong Chin Su offered laboratory assistance. The authors are grateful for their support.

[1]M. Niinomi, Sci. Technol. Adv. Mater. **4**, 445 (2003).
[2]D. D. Deligianni, N. Katsala, S. Ladas, D. Sotiropoulou, J. Amedee, and Y. F. Missirlis, Biomaterials **22**, 1241 (2001).
[3]T. M. Lee, R. S. Tsai, E. Chang, C. Y. Yang, and M. R. Yang, J. Mater. Sci.: Mater. Med. **13**, 341 (2002).
[4]C. Buzea, I. I. Pacheco, and K. Robbie, Biointerphases **2**, MR17 (2007).
[5]H. J. Kim *et al*., J. Biomed. Mater. Res. Part A **74**, 366 (2005).
[6]X. Liu, P. K. Chu, and C. Ding, Mater. Sci. Eng. R. **47**, 49 (2004).
[7]S. Rupprecht, A. Bloch-Birkholz, B. Lethaus, F. W. Neukam, and A. Schlegel, Clin. Oral Implants Res. **16**, 98 (2005).
[8]A. Balamurugan, A. H. S. Rebelo, S. Kannan, J. M. F. Ferreira, J. Michel, G. Balossier, and S. Rajeswari, J. Biomed. Mater. Res. Part B. **81**, 441 (2007).
[9]J. E. Raynor, J. R. Capadona, D. M. Collard, T. A. Petrie, and A. J. García, Biointerphases. **4**, FA3 (2009).
[10]Y. R. Yang, R. Glover, and J. L. Ong, Colloids Surf., B **30**, 291 (2003).
[11]V. Perla and T. J. Webster, J. Biomed. Mater. Res. Part A **75**, 356 (2005).
[12]K. Y. Cai, J. Bossert, and K. D. Jandt, Colloids Surf., B **49**, 136 (2006).
[13]C. C. Wang, Y. C. Hsu, S. C. Lu, and T. M. Lee, J. Biomed. Mater. Res. Part A **88**, 370 (2009).
[14]Technical Documents Department, *NanoScope Command Reference Manual* (Digital Instruments, CA, 1996), Chap. 12, pp. 87–88.
[15]F. Mabboux, L. Ponsonnet, J. J. Morrier. N. Jaffrezic, and O. Barsotti, Colloids Surf., B **39**, 199 (2004).
[16]J. Lawrence, L. Hao, and H. R. Chew, Surf. Coat. Technol. **200**, 5581 (2006).

[17]W. Zhou *et al*., Surf. Coat. Technol. **200**, 6155 (2006).
[18]A. V. Bandura, D. G. Sykes, V. Shapovalov, T. N. Troung, J. D. Kubicki, and R. A. Evarestov, J. Phys. Chem. B **108**, 7844 (2004).
[19]L. Ponsonnet, V. Comte, A. Othmane, C. Lagneau, M. Charbonnier, M. Lissac, and N. Jaffrezic, Mater. Sci. Eng., C **21**, 157 (2002).
[20]M. J. Chen, C. Y. Wur, D. P. Song, W. M. Dong, and K. Li, J. Mater. Sci: Mater. Med. **20**, 1831 (2009).
[21]K. Webb, V. Hlady, and P. A. Tresco, J. Biomed. Mater. Res. **41**, 422 (1998).
[22]T. A. Horbett, J. J. Waldburger, B. D. Ratner, and A. S. Hoffman, J. Biomed. Mater. Res. **22**, 383 (1988).
[23]G. Sagvolden, I. Giaever, E. O. Pettersen, and J. Feder, Proc. Natl. Acad. Sci. U.S.A. **96**, 471 (1999).
[24]G. Sagvolden, Biophys. J. **77**, 526 (1999).
[25]B. Feng, J. Y. Chen, S. K. Qi, L. He, J. Z. Zhao, and X. D. Zhang, J. Mater. Sci.: Mater. Med. **13**, 457 (2002).
[26]L. Ponsonnet, K. Reybier, N. Jaffrezic, V. Comte, C. Lagneau, M. Lissac, and C. Martelet, Mater. Sci. Eng., C **23**, 551 (2003).